A manganese (II)-based coordinative dendrimer with robust efficiency in intracellular peptide delivery

Lanfang Ren [a], Yang Gao [b,**], Yiyun Cheng [a,*]

[a] Shanghai Key Laboratory of Regulatory Biology, School of Life Sciences, East China Normal University, Shanghai, 200241, China
[b] College of Physics and Optoelectronic Engineering, Shenzhen University, Shenzhen, 518060, China

ARTICLE INFO

ABSTRACT

Peptides have gained increasing interests as drug candidates in modern pharmaceutical industry, however, the development of peptide drugs acting on intracellular targets is limited due to their membrane impermeability. Here, we reported the use of metal-terpyridine based coordinative dendrimer for cytosolic peptide delivery. Among the investigated transition metal ions, Mn^{2+}-coordinated polymer showed the highest delivery efficiency due to balanced peptide binding and release. It showed robust efficiency in the delivery of peptides with different charge property and hydrophobicity into various primary cells. The efficiency of Mn^{2+}-terpyridine based polymer is superior to cell penetrating peptides such as oligoarginines. The material also delivered an autophagy-inducing peptide derived from Beclin-1 into cells and efficiently induced autophagy in the cells. This study provides a promising alternative to cell penetrating peptides for cytosolic peptide delivery.

1. Introduction

Peptides are attractive drug candidates due to their benefits such as high potency and selectivity, biocompatibility and good aqueous solubility compared to traditional small-molecule drugs [1–4]. It is reported that more than 10% FDA approved drugs are peptides. Up to now, more than a hundred peptide drugs entered into markets for clinical use, and there are still hundreds of peptide candidates being evaluated at different stages of clinical trials [5]. Though achieved promising performance in medical industry, peptide drugs have met several challenges. First, peptides are easily degraded due to their chemical nature. There are hundreds of proteases in our body that are capable of degrading peptides. As a result, peptide drugs usually possess short life-times, and need carriers or supramolecular assembly strategies to protect them against enzyme degradation. Second, the currently approved peptide drugs are mainly acting on extracellular targets. It is difficult to translate peptides that require cell membrane penetration into clinics due to their membrane impermeability [6]. The development of vehicles that can efficiently deliver cargo peptides inside living cells is highly desired [7,8].

A major method to improve the membrane permeability of peptides is using cell-penetrating peptides (CPPs) [9–12]. CPPs such as HIV-1 transactivator of transcription (TAT) and oligoarginines (i.e. R8 and R9) were usually covalently fused to the N- or C- terminus of cargo peptides to facilitate their cell internalization. However, the fusion of CPPs on cargo peptides cannot improve their stability against proteases. In addition, the CPP-fused peptides are usually entrapped in acidic compartments after endocytosis and will be degraded by lysosomal enzymes due to limited endolysosome escape. Besides CPP techniques, cargo peptides were covalently or non-covalently attached to membrane permeable nanoparticles or polymers for improved proteolytic stability and intracellular delivery. For example, thiol-terminated peptides were conjugated to inorganic nanoparticles via thiol-metal bond for peptide drug delivery [13–17]. Various therapeutic peptides were covalently conjugated to cationic polymers via biodegradable linkages or enzyme-sensitive peptide spacers for the same purpose [18–22]. Moreover, peptides were fabricated into different nanostructures to increase proteolytic stability and cytosolic delivery efficiency [23–28]. A hydrophobic and lipophobic fluorous tag was decorated on peptide terminate, and the conjugate was further assembled into nanoparticles for efficient intracellular delivery both in vitro and in vivo [29]. Peptide segments were engineered into activatable protein nanoparticles via

pairwise coiled-coil dimerization, and the nanoparticles were internalized into target cells, followed by the enzyme cleavage of peptide linkers and the sustained release of cargo peptides [5]. These covalent strategies are usually involved with complicated synthesis and peptide modification before cytosolic delivery.

In an alternative strategy, anionic polymers such as poly(propylacrylic acid) were co-assembled with cationic peptides into nanoparticles via non-covalent ionic interactions for improved stability and intracellular delivery [30,31]. This strategy is only applicable to oppositely charged peptides. Besides, several polymers grafted with ligands such as guanidinium, boronic acid, and fluoroalkyls were proposed to deliver proteins and peptides via non-covalent interactions [32–39]. Considering that cargo biomolecules have all kinds of charge and hydrophobicity properties, the design of materials with robust efficiency in cytosolic peptide delivery is challenging.

To achieve robust peptide delivery, the carriers should have strong binding affinity with different kinds of cargo peptides [40,41]. Immobilized metal affinity chromatography (IMAC) is a technique widely used to separate biomolecules such as proteins and peptides [42]. The method is based on interfacial interactions of biomolecules with immobilized metal ions. Generally, the immobilized metal ion such as zinc ion (Zn^{2+}) has high binding affinity with various amino acids such as histidine, cysteine, methionine, aspartic acid, glutamic acid via coordination or ionic interactions. Inspired by the IMAC technique, we can develop a family of coordinative polymers for cytosolic biomolecule delivery by grafting chelating ligands onto polymers, followed with metal coordination. Our previous study showed that dipicolylamine/Zn^{2+} grafted polymers can be used to deliver proteins and peptides into living cells [43]. In this study, we reported a Mn^{2+}/terpyridine (TPy) based polymer for robust delivery of peptides into various kinds of cells (Scheme 1). TPy is a tridentate *N,N,N*-type pincer ligand widely used in supramolecular chemistry, catalysis and chemical biology [44–47]. TPy can form stable mono-TPy (1:1) and bis-TPy (2:1) complexes with transition metal ions [48]. Here, TPy was grafted on a cationic polymer, and then coordinated with transition metal ions including Mn^{2+}, Fe^{2+}, Co^{2+}, Ni^{2+}, Cu^{2+} and Zn^{2+} to prepare coordinative polymers. A generation 5 polyamidoamine (PAMAM) dendrimer (G5 dendrimer) was used as the polymer scaffold [49–53]. The prepared polymers were then used as carrier to deliver various kinds of cargo peptides into living cells.

2. Experimental section

2.1. Materials

2,2':6',2''-terpyridine-4'-carbaldehyde was purchased from Alfa (Zhengzhou, China). G5 PAMAM dendrimer was purchased from Dendritech (Midland, USA). NaBH$_3$CN was obtained from J&K Scientific (Shanghai, China). Bovine serum albumin (BSA), MnCl$_2$, NiCl$_2$·6H$_2$O and CuCl$_2$·2H$_2$O were purchased from Sigma-Aldrich (St. Louis, USA). FeCl$_2$·4H$_2$O, CoCl$_2$·6H$_2$O and ZnCl$_2$ were purchased from Aladdin (Shanghai, China). All the peptides were purchased from GL Biochem. (Shanghai, China). Anti-LC3B, anti-p62, anti-GAPDH and Goat anti-rabbit Alexa Fluor®680 secondary antibodies were purchased from Abcam (Cambridge, UK). MTT was obtained from Sangon Biotech. (Shanghai, China). Trypan blue was obtained from Yesen (Shanghai, China). TransExcellent™ (TransEx) was obtained from Cenji Biotech. (Shanghai, China).

2.2. Synthesis and characterization of coordinative polymers

TPy was dissolved in methanol and reacted with G5 dendrimer at a feeding molar ratio of 37:1 in anhydrous methanol. After stirring at 4 °C for 22 h, the reaction solutions were added with NaBH$_3$CN (2 mol equivalents of TPy), and stirred for another 2 h. The obtained products were intensively dialyzed against methanol and deionized water and freeze-dried for further characterization. The average number of TPy conjugated on each G5 dendrimer (G5-TPy, defined as GT) was characterized by ^{1}H NMR spectroscopy (Bruker, 500 MHz, 4 mg/mL in D$_2$O). Transition metal ions (M^{2+}) including Mn^{2+}, Fe^{2+}, Co^{2+}, Ni^{2+}, Cu^{2+} and Zn^{2+} were dissolved in methanol. The metal ion solutions were then complexed with TPy-grafted polymers in methanol at a M^{2+}/TPy molar ratio of 1:1. The mixtures were stirred at room temperature for 3 h, followed by drying under vacuum to obtain GT/M^{2+} chelates. The products were termed GT/Mn^{2+}, GT/Fe^{2+}, GT/Co^{2+}, GT/Ni^{2+}, GT/Cu^{2+} and GT/Zn^{2+}, respectively. Other G5-TPy conjugates synthesized at TPy/G5 dendrimer feeding molar ratios of 30:1, 60:1 and 90:1 (defined as GTx, x is equal to average number of TPy conjugated on each G5) were prepared by similar procedures and characterized by ^{1}H NMR spectroscopy. The hydrodynamic size of the prepared coordinative polymers was measured by dynamic light scattering (DLS) (Zetasizer Nano ZS 90, Malvern). For the spectrophotometric titration assay, metal ion solutions (1.0 mg/mL) were added into the GT solution in methanol at M^{2+}/TPy feeding molar ratios ranging from 0.1:1 to 1:1. The
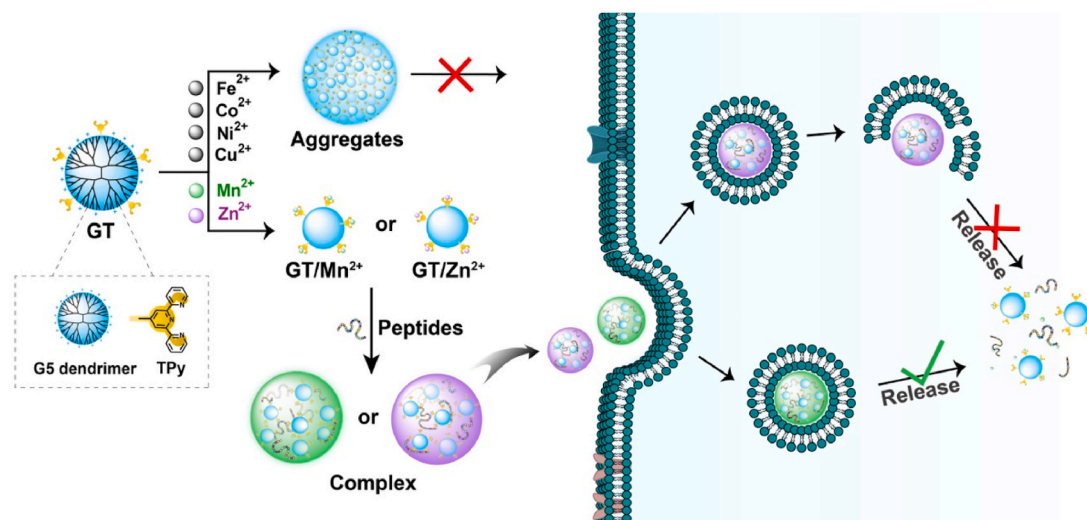
Scheme 1. GT/M^{2+} coordinative polymers for cytosolic peptide delivery. GT/Mn^{2+} showed the highest efficiency in the delivery of cargo peptides with different properties into cytosol of living cells.

concentration of GT polymer was 40 μg/mL and the final volume of solutions was fixed at 1.0 mL. After 30 min, the absorbances (Abs) of the complex solutions ranging from 200 to 800 nm were recorded by a spectrophotometer (Cary 60 UV–Vis, Agilent Technologies) at room temperature. The modification of TPy moieties to G5 dendrimers and the formation of metal complexes were also characterized by Fourier infrared spectrometry (FT-IR) (Nicolet iS10, Thermo Scientific, USA) and X-ray photoelectron spectroscopy (XPS) (K-Alpha, Thermo Scientific, USA). The XPS data were processed and fitted by Thermo Avantage software.

2.3. Synthesis of fluorescent dye-labeled GT

GT was dissolved in deionized water, and rhodamine B isothiocyanate (RBITC) was dissolved in DMSO. Then RBITC was added into the GT solution at a RBITC/GT molar ratio of 3:1. The mixture solution was stirred in dark for 24 h at room temperature. The products were intensively dialyzed against 1x phosphate buffer saline (PBS) solution and deionized water. The obtained sample GT-RBITC was freeze-dried for further use. The GT-RBITC/Mn^{2+} and GT-RBITC/Zn^{2+} chelates were prepared according to the procedure describe above.

2.4. Preparation and characterization of polymer/peptide complexes

The peptides were conjugated with fluorescein isothiocyanate (FITC) at the *N*-terminus via a 6-aminocaproic acid spacer during peptide synthesis. These FITC-labeled cargo peptides with different isoelectric points (pI), charge and kyto-doolittle hydrophobicity (Kd) values were arranged and named in a statistical table. GT, GT/Mn^{2+} and GT/Zn^{2+} were mixed with cargo peptides in 100 μL deionized water at room temperature. After incubation for 30 min, the prepared polymer/peptide complexes were further diluted with 150 μL deionized water. The final concentrations of peptides and polymers were 10 μM and 0.5 μM, respectively. The particle size and morphology of the formed complexes were characterized by DLS (Zetasizer Nano ZS 90, Malvern) and transmission electron microscopy (TEM, HT7700, Hitachi) at an acceleration voltage of 100.0 kV. The fluorescence spectra of the complex solutions were measured by a fluorescence spectroscopy (Hitachi F-4500, Japan). The samples were recorded from 480 to 700 nm under the excitation wavelength of 450 nm at room temperature. The fluorescence intensity was measured in deionized water or in the presence of 0.1 mg/mL BSA. Free peptides at an equal concentration were tested as controls.

2.5. Cell culture and cytosolic peptide delivery

HeLa cells, HeLa cells stably expressing GFP-LC3 and NIH3T3 cells were grown in Dulbecco's modified Eagle's medium (DMEM, Gibco) supplemented with 10% (v/v) fetal bovine serum (FBS, Gemini). BAT and iWAT cells were cultured in DMEM containing 20% FBS (Gemini). RAW264.7 cells and MEF primary cells were incubated in DMEM (Gibco) containing 10% FBS (Gibco). MSC cells were grown in α-MEM (Gibco) containing 10% FBS (Gibco). IMCD3 cell lines were incubated in DMEM-F12 (Hyclone) containing 10% FBS (Gibco). iPS cells were incubated in mTeSR™ (STEMCELL) with Matrigel (Corning) pre-coated culture dishes. CD8$^+$ T cells were grown in RPMI 1640 culture medium. HUDEP2 cells were cultured in serum-free expansion medium (STEMCELL) containing needed cytokines.

The cargo peptides were complexed with the coordinative polymers as described above. The complexes were diluted with 100 μL serum-free culture medium and statically incubated for 30 min. The solutions were further diluted by another 150 μL serum-free medium. Cells were grown in 48-well plates overnight before cytosolic peptide delivery. At ~90% confluence, the cells were incubated with the above 250 μL complex solutions for 4 h. Before analyzing by flow cytometry using BD LSRFortessa (USA), the cells were treated with trypan blue (0.04%, w/w) to quench the extracellular fluorescence, and then washed by PBS

twice. For confocal imaging, the cells were pre-transferred to confocal dishes overnight (90% confluence). The doses of polymer and peptide, as well as the volume of culture media were enlarged 4-fold compared to those used in 48-well plate experiments. The cells were incubated and washed by the same procedure as described above and then observed by laser scanning confocal microscopy (LSCM, Leica SP5, Germany). Free peptides, octaarginine R8-conjugated peptides, TransEx and a bronated dendrimer GP were tested as controls. To investigate the intracellular trafficking of polymers and peptides after endocytosis, HeLa cells were incubated with the complexes consisting of FITC-labeled peptides and RBITC-labeled GT/Mn^{2+} or GT/Zn^{2+} for 2–4 h before analyzing by flow cytometry and observation by LSCM. The concentrations of cargo peptides P1–P21 were fixed at 10 μM. As to verify the cell internalization of Beclin-1 (Bec 1), HeLa cells at 60% confluence were treated with Bec 1, GT/Mn^{2+}/Bec 1 and Bec 1-TAT, respectively, and replaced with 200 μL fresh medium containing 10% FBS at 4 h. After another 20 h culture, the cells were washed and analyzed by flow cytometry and confocal microscopy as mentioned above. The concentrations of Bec 1 and Bec 1-TAT were tested at 10 μM and 40 μM. The concentration of polymer in cytosolic peptide delivery experiments was 0.5 μM.

2.6. Cell viability and hemolysis assay

HeLa cells were seeded in 96-well plates for overnight. At ~90% confluence, the cells were treated with 100 μL serum-free medium containing different concentrations of polymers (16, 20, and 24 μg/mL, respectively. 20 μg/mL is the polymer concentration used in peptide delivery experiments). After 4 h incubation, the culture media were replaced with 100 μL fresh medium containing 10% FBS. The cells were further cultured for 20 h, followed by a standard MTT assay.

For hemolysis assay, the whole blood collected from BALB/c mice was added into centrifugal tubes in the presence of 100 μL of heparin sodium solution (1.0 mg/mL in PBS). The blood was diluted with PBS (pH 7.4) and centrifuged at 2000 rpm for 5 min. The supernatant was refreshed, and the sample was further centrifuged for several times until the supernatant turned colorless. The final sediment was re-suspended in PBS. GT, GT/Mn^{2+} or GT/Zn^{2+} was added into the suspension at a concentration of 0.5 μM, which was equal to the dose used in peptide delivery experiments. PBS and Triton-100 (TX-100, 1/200, v/v) were tested as negative and positive controls, respectively. The tubes were statically cultured for 1 h at 37 °C. After centrifugation at 2000 rpm for 5 min, the supernatants were collected, and the absorbances of the samples at 540 nm were measured by a microplate reader (Multiskan GO, Thermo scientific). The hemolysis ratio was calculated by the equation: $(A_{sample}-A_{PBS})/(A_{TX-100}-A_{PBS}) \times 100\%$. Where A_{sample}, A_{PBS} and A_{TX-100} are the absorbances of samples treated with GT, GT/Mn^{2+}, GT/Zn^{2+}, negative and positive controls, respectively.

2.7. Autophagy assay

HeLa cells or HeLa cells stably expressing GFP-LC3 at 60% confluence were treated with Bec 1, GT/Mn^{2+}, GT/Mn^{2+}/Bec 1 and Bec 1-TAT, respectively. The concentrations of Bec 1 and Bec 1-TAT were tested at 10 μM and 40 μM. The concentration of GT/Mn^{2+} was fixed at 0.5 μM. The cells were treated with the samples for 4 h, and then the culture media were removed and replaced with 200 μL fresh medium containing 10% FBS. After that, the cells were further cultured for 20 h. HeLa (GFP-LC3) cells were rinsed with PBS twice and observed by LSCM. The average number of GFP-LC3 puncta per cell was counted and calculated by the NIH ImageJ software. HeLa cells treated with the samples were also rinsed with PBS and then stained with AO (8 μg/mL) in 1.0 mL DMEM for 5 min. Then the cells were washed with PBS and observed by LSCM.

2.8. Western blotting assay

HeLa cells were seeded in 6-well plates and treated with Bec 1, GT/Mn^{2+}, GT/Mn^{2+}/Bec 1 and Bec 1-TAT as described above. After treatment, the cells were rinsed with PBS and lysed by 1x protein loading buffer (Epizyme biotech., China) on ice for 30 min. The proteins in the lysate were denatured by heating the samples at 100 °C for 10 min. After that, the samples were subjected to sodium dodecyl sulfate-polyacrylamide gel electrophoresis (SDS-PAGE) and immunoblotted with a nitrocellulose (NC) membrane. The NC membrane was blocked by 5% non-fat milk (wt/v, PBS) for 1 h and washed with PBS for three times, and incubated with primary antibodies overnight at 4 °C. The antibodies anti-LC3B, anti-p62 and anti-GAPDH were diluted by 1:3000 (v/v), 1:5000 (v/v) and 1:5000 (v/v) in primary antibody dilution buffer (Sangon Bio.), respectively. The membrane was then washed with Tris Buffered Saline with Tween (TBST, 0.1% (v/v) Tween 20), and incubated with secondary antibody (1:10000 (v/v), 3% BSA solution) in dark for 1 h at room temperature. Finally, the membrane was rinsed with TBST and scanned on an Odyssey CLx infrared imaging system (LI-COR, USA). Commercial pre-dyed protein marker (Epizyme biotech., China) was used to indicate the target proteins.

3. Results

3.1. Synthesis and characterization of GT and its metal chelates

The metal chelating agent 2,2':6',2''-terpyridine-4'-carbaldehyde was directly reacted with amine-terminated G5 PAMAM dendrimer through Schiff base reaction, followed by the reduction of yielding C=N bond using sodium cyanoborohydride (NaBH$_3$CN). The obtained product G5-TPy (GT) conjugate was characterized by ^{1}H NMR, and the average number of TPy ligands grafted on each dendrimer was calculated to be 33 (Figure S1). The polymer was then complexed with transition metal ions M^{2+} including Mn^{2+}, Fe^{2+}, Co^{2+}, Ni^{2+}, Cu^{2+} and Zn^{2+} in methanol to prepare metal chelates. GT was firstly titrated with

M^{2+} at different metal ion to TPy molar ratios. UV–Vis spectrum was used to analyze the coordination of metal ions to TPy moieties on GT (Figure S2). For GT, an absorption peak at about 280 nm was observed, which is attributed to the π-π* transition of TPy moieties. After the addition of M^{2+}, an obvious bathochromic shift of the band to about 340 nm was found for all the M^{2+} (Fig. 1a). For the Fe^{2+}/GT chelate, peaks for the metal-centered (MC) band and the metal-to-ligand charge transfer (MLCT) band were also observed (Figure S2b) [54]. These results are in well accordance with those reported in the references [55–57]. The change of the lowest absorption band at 340 nm was plotted as a function of M^{2+}/TPy molar ratio. With increasing M^{2+}/TPy molar ratio from 0:1 to 1:1, the absorption band at 340 nm firstly increased, and then stayed the same above a critical ratio for Fe^{2+}, Co^{2+}, Ni^{2+}, Cu^{2+} and Zn^{2+} ions. This result suggested that the coordination of TPy with these metal ions was saturated above this ratio. In addition, the band at 280 nm exhibited obvious hypsochromic shift after the addition of these metal ions, due to the formation of TPy:M^{2+}:TPy complex (1:2). For Mn^{2+}/GT, the band at 340 nm was gradually increased within the investigated Mn^{2+}/TPy molar ratios, while the band at 280 nm was only slightly shifted during the titration, suggesting the formation of Mn^{2+}:TPy complex (1:1). A Job's plot was further performed to analyze the binding stoichiometry between GT and M^{2+} (Fig. 1b). It indicated that the stoichiometry of complexation between metal ions and TPy on GT was 1:1 for Mn^{2+} and 2:1 for other metal ions [58]. The results confirmed that Fe^{2+}, Co^{2+}, Ni^{2+}, Cu^{2+} and Zn^{2+} have stronger binding affinity with GT than Mn^{2+}.

The modification of TPy moieties to G5 dendrimers and the formation of metal complexes were further verified by FT-IR and XPS. As the FT-IR spectra shown at Figure S3, the peaks at 3271.64 cm^{-1} and 1632.45 cm^{-1} are attributed to amide vibration, and the bands appeared at 2930.31 cm^{-1} and 1539.88 cm^{-1} are assigned to –CH$_2$- bending vibration [59]. The peak at 1407.30 cm^{-1} for terpyridine-modified polymer GT is attributed to the broad vibration of C=N bond in the pyridine moieties [60]. Another feature of the pyridine moieties is the band at 792.12 cm^{-1} for the C–C bond [61]. In the spectrum of GT/Mn^{2+}, the
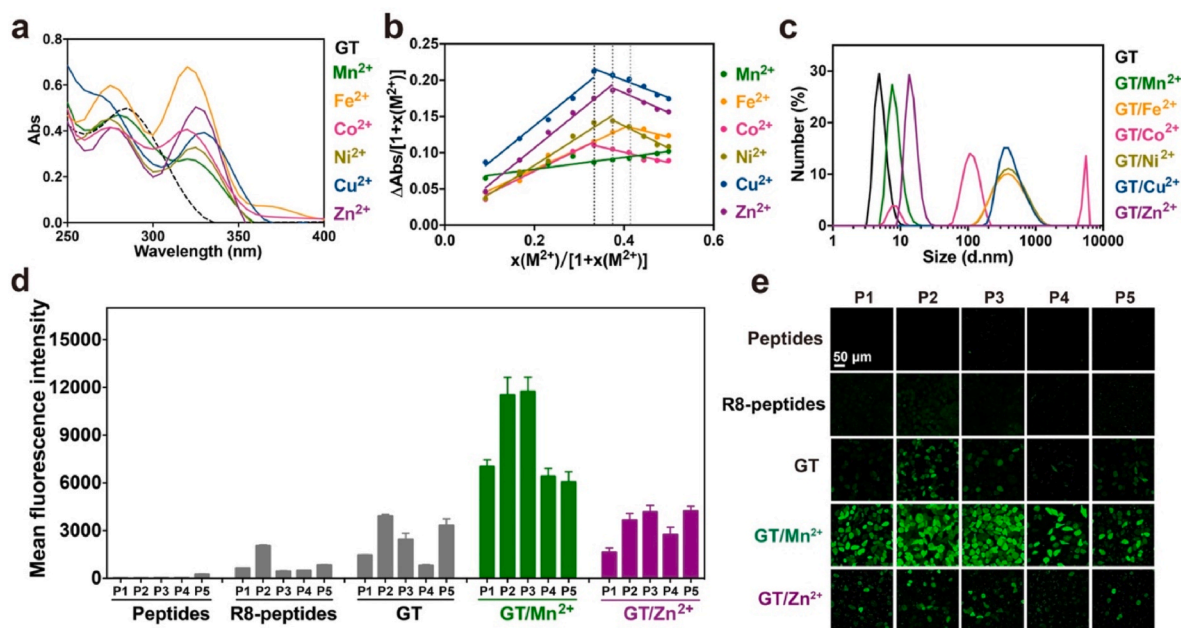

Fig. 1. Characterization of coordination polymer GT/M^{2+} and their efficiency in cytosolic peptide delivery. (a) UV–Vis spectra of GT and GT/M^{2+} complexes prepared at a M^{2+}/TPy molar ratio of 1:1 in methanol. (b) Job's plots of GT/M^{2+} coordination polymers in methanol. The x(M^{2+}) was defined as the M^{2+}:TPy molar ratio, while the △Abs was equal to the absorbance of GT/M^{2+} polymers minus that of free GT in methanol. (c) Size distribution of GT and GT/M^{2+} complexes in deionized water. Mean fluorescence intensity (d) and confocal images (e) of HeLa cells treated with GT, GT/Mn^{2+} and GT/Zn^{2+} complexes with five cargo peptides, respectively. Free peptides and R8-conjugated peptides were tested as negative and positive controls, respectively. The doses of peptide and polymer were fixed at 10 μM and 0.5 μM, respectively. Data were shown as mean ± standard deviation (s.d., n = 3).

absorption bands at 1427.55 cm^{-1} and 794.05 cm^{-1} ascribed to the terpyridine moieties were shifted to higher wavenumbers compared to those of GT, suggesting the coordination of terpyridine with Mn^{2+} ions in the formed complex. According to the XPS spectra shown at Figure S4, the main elements in GT polymers were C, N and O, and the signal of Mn^{2+} appeared after coordination [62]. The Mn 2p spectra of MnCl$_2$ were deconvoluted into four photoelectron peaks at 641.21, 642.40, 646.91 and 653.55 eV, respectively, while the nitrogen atoms in GT showed two peaks at 398.34 eV and 400.49 eV, which were assigned to N–H and C=N, respectively. After Mn^{2+} coordination, the four Mn 2p peaks were shifted to lower binding energies (Figure S5a-S5b), and the N 1s peaks on GT were shifted to higher binding energies at 398.50 and 400.63 eV, respectively, due to the donation of electrons from terpyridine or amine moieties to Mn^{2+} (Figure S5c-S5d) [63,64]. These results suggested the successful coordination of Mn^{2+} with GT.

In later studies, we fixed the molar ratio of metal ions to TPy at 1:1. The samples were prepared in methanol, the solvents in the complex solution were removed by evaporation, and the complexes were further dissolved in deionized water. It is observed that the Mn^{2+} and Zn^{2+} complexes are fully soluble in deionized water, while the Fe^{2+}, Co^{2+}, Ni^{2+} and Cu^{2+} complexes yielded partial precipitates. Dynamic light scattering (DLS) measurement showed that the sizes of GT, GT/Mn^{2+} and GT/Zn^{2+} in deionized water are around 10 nm, while the Fe^{2+}, Co^{2+}, Ni^{2+} and Cu^{2+} chelates are detected with large aggregates (Fig. 1c). The results supported the formation of TPy:M^{2+}:TPy complexes for Fe^{2+}, Co^{2+}, Ni^{2+}, and Cu^{2+} chelates, yielding crosslinked nanoclusters and finally insoluble aggregates in aqueous solution. We therefore only investigated the GT/Mn^{2+} and GT/Zn^{2+} polymers in further peptide delivery experiments.

3.2. Cytosolic peptide delivery by GT/Mn^{2+} and GT/Zn^{2+} complexes

The cargo peptides used in the study were shown in Table 1. P1–P5 with distinct charge properties were firstly investigated as the model peptides. The coordinative polymers GT/Mn^{2+} and GT/Zn^{2+} were mixed with the peptides for 30 min before cytosolic delivery. As shown at Fig. 1d-e, GT/Mn^{2+} displayed the highest efficiency in the delivery of P1–P5 among the investigated materials as well as CPP octaarginine (R8)-conjugated peptides. Additionally, the commercial reagent TransEx and a previously reported polymer GP were used as positive controls [32,33]. As shown at Figure S6, GT/Mn^{2+} showed comparable peptide delivery efficiencies to TransEx and GP. We further investigated why GT/Mn^{2+} has superior efficiency to GT/Zn^{2+} in peptide delivery. As shown at Fig. 2a-b, the polymers of GT, GT/Mn^{2+} and GT/Zn^{2+} showed low cytotoxicity and hemolytic toxicity at the concentrations used in peptide delivery experiments (10 μM and 0.5 μM for peptides and polymers, respectively). DLS and TEM results showed that both GT/Mn^{2+} and GT/Zn^{2+} formed uniform nanoparticles with P1–P5 in aqueous solutions (Fig. 2c and S7).

Additionally, the coordinative polymer GT/Mn^{2+} showed a relatively high relaxation rate (4.39 mM^{-1}s^{-1}) [65–67], suggesting its

potential use as a magnetic resonance imaging (MRI) contrast (Fig. 2d-e). The TPy grafting ratio on G5 dendrimer may influence the peptide delivery efficiency and cytotoxicity of the coordinative polymers GT/Mn^{2+}. In this case, we also synthesized a series of G5-TPy conjugates with different TPy grafting numbers other than 33. By varying the feeding ratio of TPy to G5, G5-TPy conjugates with average numbers of 27, 58 and 83 TPy were obtained (the products were termed GT$_{27}$, GT$_{58}$ and GT$_{83}$, respectively, Figure S8). Among all the synthesized conjugates, GT/Mn^{2+} with 33 TPy moieties and GT$_{58}$/Mn^{2+} with 58 TPy moieties showed relatively higher peptide delivery efficiency (Figure S9a-S9b). However, the conjugates with higher TPy grafting ratios such as GT$_{58}$/Mn^{2+} were observed with higher cytotoxcity on the treated cells than GT$_{27}$/Mn^{2+} and GT$_{33}$/Mn^{2+} (Figure S9c-S9d). Based on both peptide delivery efficiency and cytotoxicity, GT/Mn^{2+} with 33 TPy moieties was selected as the lead material in this study.

Next, we investigated the reason why GT/Mn^{2+} has superior efficiency to GT/Zn^{2+} in cytosolic peptide delivery. We visualized the intracellular trafficking of both coordinative polymers and their complexes with cargo peptides by confocal microscope. GT was labeled with rhodamine B isothiocyanate (RBITC), a red fluorescent dye, and further complexed with metal ions. The results showed that both the polymers of GT-RBITC/Mn^{2+} and GT-RBITC/Zn^{2+} could be efficiently internalized by the cells (Fig. 3a-b). After peptide complexation with the RBITC-labeled polymers GT/Mn^{2+} and GT/Zn^{2+}, the red fluorescence also showed no significant difference in cytosols of cells (Figure S10a). However, most FITC-labeled peptides were co-localized with GT/Zn^{2+} after endocytosis (Fig. 3c and S10b). Punctate yellow dots were observed in the treated cells during 4 h incubation. In comparison, the peptides delivered by GT/Mn^{2+} were distributed the green fluorescence throughout the cells, suggesting sufficient peptide release from the polymer matrix. The results indicated that GT/Zn^{2+} has difficulty in releasing the bound peptides after internalization. To confirm this hypothesis, we investigated the peptide release from both polymers triggered by an anionic protein bovine serum albumin (BSA), which mimics the abundant proteins in the cytosol. It's observed that the fluorescence from all the five FITC-conjugated peptides was quenched after complexation with GT/Mn^{2+} and GT/Zn^{2+}, which is due to the formation of polymer/peptide nanoparticles. Compared to GT/Mn^{2+}, GT/Zn^{2+} showed higher efficiency in quenching the fluorescence from FITC-conjugated peptides, suggesting the formation of more congested complexes (Fig. 3d and S10c). In the presence of BSA, the quenched fluorescence for both complexes was partially recovered due to the competitive binding of BSA with GT/M^{2+} via ionic interactions. However, the fluorescence recovery for GT/Zn^{2+} was less obvious than that for GT/Mn^{2+}. These results clearly proved that the low efficiency of GT/Zn^{2+} in cytosolic peptide delivery is attributed to poor peptide release after delivery.

3.3. Robustness of cytosolic peptide delivery by GT/Mn^{2+} polymer

We further investigated the complexation of GT/Mn^{2+} with different

Table 1
The model peptides with different properties.

Peptides	Sequence	Charge	Kd	pI	Peptides	Sequence	Charge	Kd	pI
P1	KTCENLADTY	−2	−9	3	P12	MHMKKVLDC	0	−0.2	7.3
P2	EERHGGFLC	−2	−6.4	4.2	P13	RPGFAPFLC	0	5.6	6.2
P3	ACSAG	−1	4.9	0.6	P14	KYGVYHPLC	0	−1.2	7.3
P4	FKSTWYMHH	0	−9.3	7.9	P15	DDKKKHHTM	0	−23.9	7.9
P5	WGGFLRKRC	2	−5.5	11.3	P16	DKKHSTMHF	0	−14.5	7.9
P6	DKAFVPEHG	−2	−7.3	4.1	P17	KAGHHHHHH	0	−21.7	9.2
P7	AVPIAQDEC	−3	2.7	0.6	P18	WGGFLRRIC	1	2.9	10.9
P8	DGVYIHPFC	−2	4	3.1	P19	YFGFRPRHA	1	−8.1	11.1
P9	REALISTIC	−1	7.6	3.3	P20	APRLRFYAC	1	0.8	9.3
P10	DRLYSFGLC	−1	2.4	3.1	P21	KHGKLFKAS	2	−7.7	10.5
P11	GLARDTIYF	−1	2.5	3.1	P22	CGVWNATFHIWHD	−2	−0.5	4.8
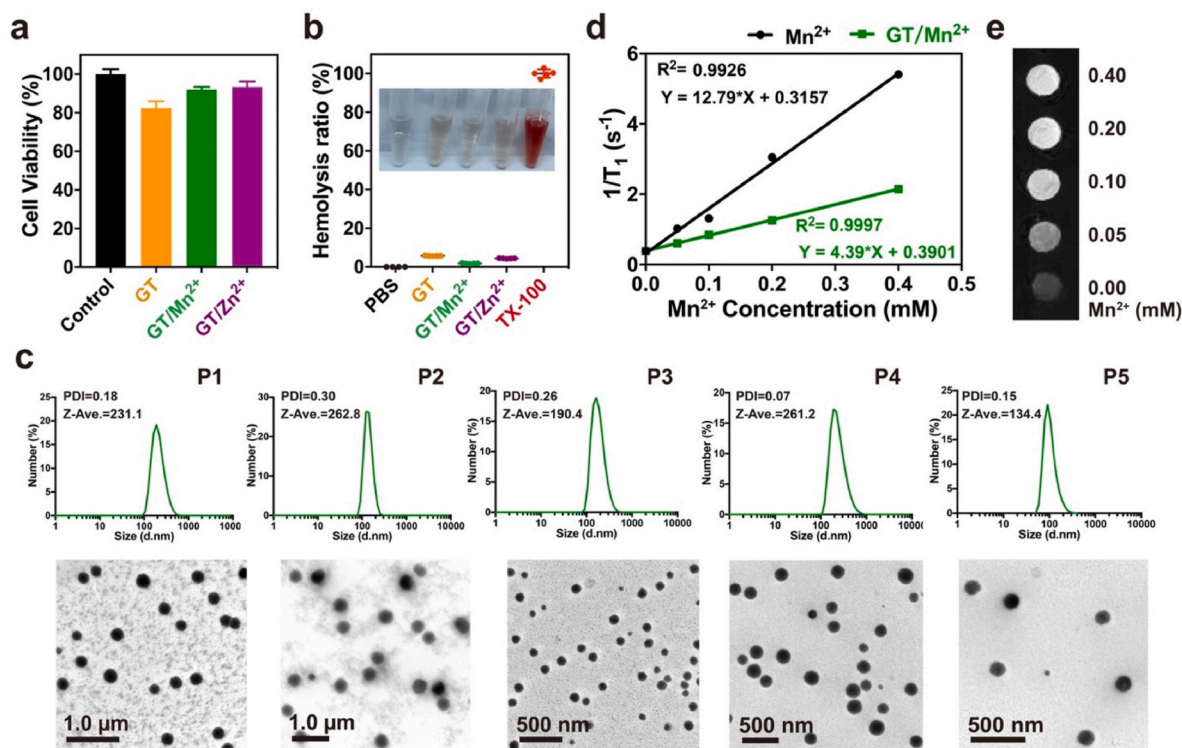
Fig. 2. Characterization of GT, GT/Mn^{2+} and GT/Zn^{2+} polymers. (a) Viability of HeLa cells treated with GT, GT/Mn^{2+} and GT/Zn^{2+} (mean ± s.d., n = 3). (b) Hemolysis activity of GT, GT/Mn^{2+} and GT/Zn^{2+} (mean ± s.d., n = 5). The polymer concentration in viability and hemolysis assays was fixed at 0.5 μM. (c) DLS measurement and TEM images of GT/Mn^{2+}/P1–P5 complexes in deionized water. The concentrations of peptides and polymers were at 2.5 μM and 0.125 μM, respectively. (d) Curve of 1/T$_1$ versus Mn^{2+} concentration for free Mn^{2+} and GT/Mn^{2+}. (e) T$_1$-weighted images of GT/Mn^{2+} at different Mn^{2+} concentrations.
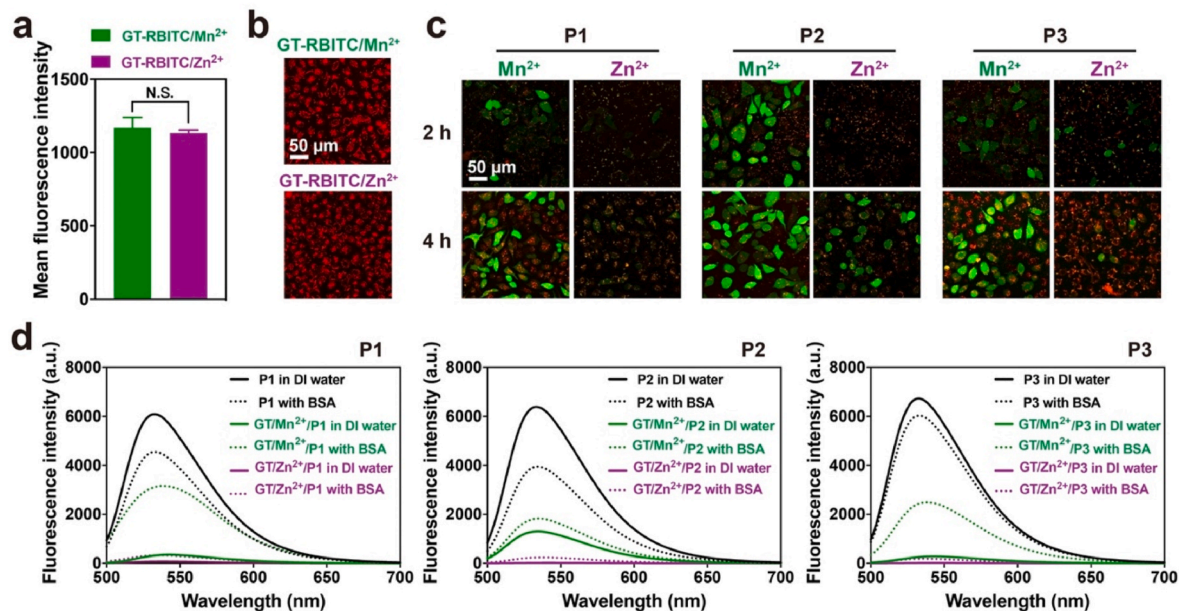

Fig. 3. Intracellular trafficking and peptide release of GT/Mn^{2+} and GT/Zn^{2+} complexes. Mean fluorescence intensity (a) and confocal images (b) of HeLa cells treated with RBITC-labeled GT/Mn^{2+} or GT/Zn^{2+}. Data were shown as mean ± s.d. (n = 3). $^{N.S.}p > 0.05$ was calculated by Students' t-test, one-tailed. (c) Confocal images of HeLa cells treated with complexes consisting of RBITC-labeled GT/Mn^{2+} or GT/Zn^{2+} and cargo peptides P1–P3 labled with FITC. The doses of peptides and polymers were 10 μM and 0.5 μM, respectively. (d) Fluorescence spectra of GT/Mn^{2+} or GT/Zn^{2+} complexes with FITC-labeled P1–P3 in deionized water and 0.1 mg/mL BSA solutions, respectively. Free peptides at a concentration of 2.5 μM in the absence and presence of 0.1 mg/mL BSA were tested as controls. The polymer concentration in the samples was 125 nM.

cargo peptides via XPS. The XPS N 1s, O 1s, C 1s, S 2p and Mn 2p spectra of peptides and GT/Mn^{2+}/peptide complexes were given in Figure S11-S16. Taken P1 (KTCENLADTY) for example, the N 1s peaks for N–H on P1 and the C=N on GT/Mn^{2+} were shifted to higher binding energies, due to the donation of electrons from amine and terpyridine to Mn^{2+} after P1 complexation with GT/Mn^{2+}, suggesting the coordination effect

of amine moieties on peptide P1 to Mn^{2+}. For C 1s spectra, we observed the peaks for C–O and C=O were decreased to lower binding energies but the one for C–C/C–N was scarcely shifted. We also confirmed that the peak of C–O shifted to lower binding energy from O 1s spectra, indicating the reaction of carboxyl groups with GT/Mn^{2+} [68]. For S 2p spectra, the peak at 166.18 eV for sulfate oxidizing from thiol group on P1 was shifted to 162.66 eV, implying the formation of Mn–S bond [69]. Similar results were observed on the XPS spectra of other cargo peptides P2–P4. These results implied that the residual groups such as amine, carboxyl, imidazole and thiol on peptides could interact with GT/Mn^{2+} in the formed complexes.

Next, we further tested the robustness of GT/Mn^{2+} in the delivery of cargo peptides P1–P5 into different cells. As shown in Fig. 4a, GT/Mn^{2+} efficiently delivered P1–P5 into the cytosols of various living cells including mouse brown adipose tissue cells (BAT), mouse inguinal white adipose tissue cells (iWAT), mouse embryo fibroblast cells NIH3T3, mouse bone marrow mesenchymal stem cells (MSC), mouse embryonic fibroblast primary cells (MEF), mouse inner medullary collecting duct cells IMCD3, human induced pluripotent stem cells (iPS), RAW264.7 (mouse leukemic monocyte macrophages), mouse CD8^{+} T lymphocytes and human umbilical cord derived erythroid progenitor cells HUDEP2. Not limited to P1–P5, GT/Mn^{2+} also efficiently delivered a list of peptides P6–P21 with different isoelectric points (pI), charge and kytodoolittle hydrophobicity values (Kd) into cytosol of HeLa cells (Fig. 4b). These results confirmed the robust efficiency of GT/Mn^{2+} in cytosolic peptide delivery.

3.4. Cytosolic delivery of autophagy inducing peptide Beclin-1

Beclin-1 is an autophagy inducer [70,71]. Bec 1 and its class III phosphatidylinositol 3-kinase (PI3K) complex containing lipid kinase subunit Vps34 and regulatory subunit Atg14 initiate the formation of autophagosome [72,73]. The microtubule-associated protein light chain I (LC3I) is then converted to its lipidated form, LC3II, which is further attached to the membrane of autophagosome. After autophagosome maturation and lysosomal fusion, the autophagosome and its contents such as the autophagy adaptor protein p62 will be degraded (Fig. 5a). The Beclin-1-derived peptide (Bec 1, sorted as P22 in Table 1) was complexed with GT/Mn^{2+} and delivered into cells to initiate autophagy. Free Bec 1 and TAT-conjugated Bec 1 were tested as negative and positive controls, respectively. Firstly, Bec 1 delivered by GT/Mn^{2+} were showed a higher internalization efficiency than TAT- Bec 1 for 24 h (Fig. 5b-c). Next, HeLa cells stably expressing green fluorescent protein-fused LC3 (GFP-LC3) were treated with Bec 1, Bec 1-TAT and GT/Mn^{2+}/Bec 1, respectively for 24 h. As shown at Fig. 5d, GT/Mn^{2+}/Bec 1 treatment induced obvious accumulation of GFP-LC3 puncta. Quantitative analysis of GFP-LC3 dots further proved significant autophagosome accumulation in the cells treated with GT/Mn^{2+}/Bec 1 complexes. The average number of green dots in the cells treated with GT/Mn^{2+}/Bec 1 is much more than those for Bec 1 and
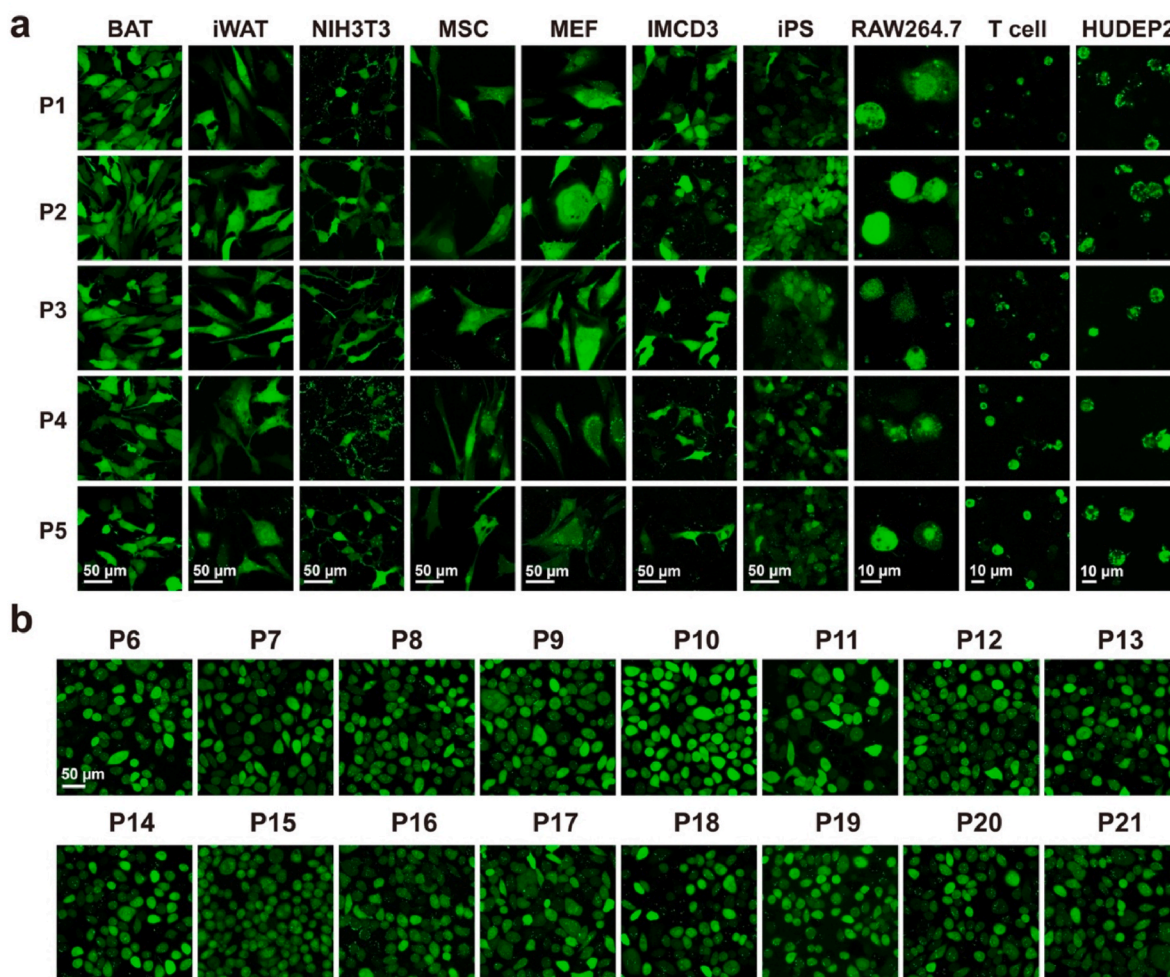

Fig. 4. Robustness of GT/Mn^{2+} in cytosolic peptide delivery. (a) Confocal images of different cells treated with GT/Mn^{2+} complexes with FITC-labeled P1–P5. (b) Confocal images of HeLa cells treated with complexes consisting of GT/Mn^{2+} and peptides P6–P21. The concentrations of peptides and GT/Mn^{2+} were fixed at 10 μM and 0.5 μM, respectively.
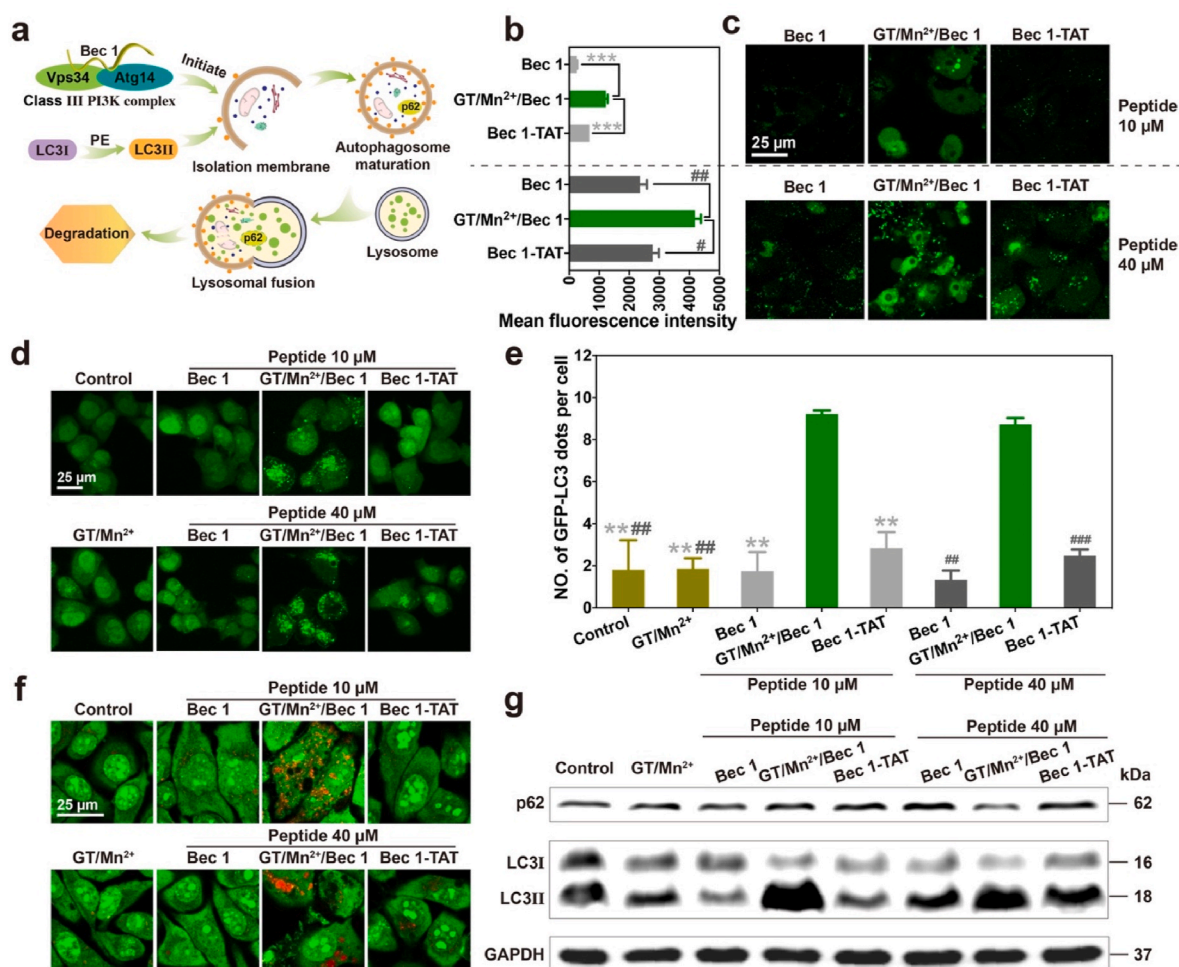
Fig. 5. GT/Mn^{2+} mediated cytosolic Bec 1 delivery to induce autophagy. (a) Schematic illustration of Bec 1-induced autophagy. Mean fluorescence intensity (b) and confocal images (c) of HeLa cells treated with Bec 1, Bec 1-TAT and GT/Mn^{2+}/Bec 1 for 24 h, respectively. Peptides were pre-labeled with FITC. Representative confocal images (d) and quantitative analysis of GFP-LC3 dots (e) in HeLa cells stably expressing GFP-LC3. The cells were treated with Bec 1, Bec 1-TAT and GT/Mn^{2+}/Bec 1, respectively for 24 h. (f) AO staining of HeLa cells treated with the Bec 1, Bec 1-TAT or GT/Mn^{2+}/Bec 1 for 24 h. (g) Western blot analysis of LC3 and p62 proteins in HeLa cells treated with Bec 1, Bec 1-TAT or GT/Mn^{2+}/Bec 1 for 24 h. The doses of peptides were 10 μM and 40 μM, respectively, and the polymer concentration was fixed at 0.5 μM. Data were shown as mean ± s.d. (n = 3). $^{\#}p < 0.05$, $^{\#\#}p < 0.01$, $^{\#\#\#}p < 0.001$, $**p < 0.01$ and $***p < 0.001$ were calculated by Students' t-test, one-tailed.

Bec 1-TAT (Fig. 5e). Acridine orange (AO) is a pH-sensitive and membrane-permeable dye. It is usually used as a probe to monitor autophagy. The autolysosomes in autophagic cells can be stained into red fluorescence by AO. Confocal images showed that HeLa cells treated with GT/Mn^{2+}/Bec 1 and further stained by AO were observed with strong red fluorescence signals [74]. In comparison, the cells treated with free Bec 1 and Bec 1-TAT were mainly observed with green fluorescence signals (Fig. 5f). Western blot analysis of the treated cells also confirmed obvious conversions of LC3I into LC3II in HeLa cells treated with GT/Mn^{2+}/Bec 1 complexes, and the autophagy adaptor protein p62 showed partial degradation under 40 μM Bec 1 (Fig. 5g). In comparison, the LC3I conversion and p62 degradation were less efficient in cells treated with free Bec 1 and Bec 1-TAT, respectively. These results proved that GT/Mn^{2+} can also efficiently deliver Bec 1 into HeLa cells and induce autophagy in the treated cells, suggesting that GT/Mn^{2+} polymers pose a great potential to be a robust carrier for the delivery of bioactive peptide drugs.

4. Conclusion

In summary, we developed a Mn^{2+}-based coordinative polymer for efficient and robust peptide delivery into living cells. The polymer

delivered a wide range of peptides with different charge and hydrophobicity properties into various cells, and showed higher potency than CPP-conjugated peptides and comparable efficiency with commercial reagent such as TransEx. In addition, the coordinative polymer delivered an autophagy inducing peptide into cells, and successfully exerted its biofunction after intracellular delivery. This study provides a promising tool for cytosolic delivery of peptides without the need of chemical modification. We may design more carriers with robust efficiency and versatile functions for peptide delivery by the proposed concept in this study. In future studies, we will tailor the chelating ligand and metal ions for balanced peptide binding and intracellular release, and investigate the potential roles of metal ions such as Mn^{2+} on the polymer in MRI imaging [75], fenton reactions for chemodynamic cancer therapy [76], and activation of cGAS-STING pathway for immunotherapy [77].

CRediT authorship contribution statement

Lanfang Ren: Conceptualization, Methodology, Data, Formal analysis, Data curation, Writing – original draft. **Yang Gao:** Resources, Writing – review & editing. **Yiyun Cheng:** Conceptualization, Writing – review & editing.

Declaration of competing interest

The authors declare that they have no known competing financial interests or personal relationships that could have appeared to influence the work reported in this paper.

Acknowledgements

Appendix A. Supplementary data

Supplementary data to this article can be found online at https://doi.org/10.1016/j.bioactmat.2021.08.006.

References

[1] D.J. Drucker, Advances in oral peptide therapeutics, Nat. Rev. Drug Discov. 19 (4) (2020) 277–289.

[2] A.P. Davenport, C.C.G. Scully, C. de Graaf, A.J.H. Brown, J.J. Maguire, Advances in therapeutic peptides targeting G protein-coupled receptors, Nat. Rev. Drug Discov. 19 (6) (2020) 389–413.

[3] Y. Wang, A.G. Cheetham, G. Angacian, H. Su, L. Xie, H. Cui, Peptide-drug conjugates as effective prodrug strategies for targeted delivery, Adv. Drug Deliv. Rev. 110–111 (2017) 112–126.

[4] X. Liu, F. Wu, Y. Ji, L. Yin, Recent advances in anti-cancer protein/peptide delivery, Bioconjugate Chem. 30 (2) (2019) 305–324.

[5] X. Yu, X. Gou, P. Wu, L. Han, D. Tian, F. Du, Z. Chen, F. Liu, G. Deng, A.T. Chen, C. Ma, J. Liu, S.M. Hashmi, X. Guo, X. Wang, H. Zhao, X. Liu, X. Zhu, K. Sheth, Q. Chen, L. Fan, J. Zhou, Activatable protein nanoparticles for targeted delivery of therapeutic peptides, Adv. Mater. 30 (7) (2018) 1705383.

[6] X. Wang, X. Bao, M. McFarland-Mancini, I. Isaacsohn, A.F. Drew, D.B. Smithrud, Investigation of the intracellular delivery of fluoresceinated peptides by a host-[2] Rotaxane, J. Am. Chem. Soc. 129 (23) (2007) 7284–7293.

[7] A.E. Rabideau, X. Liao, B.L. Pentelute, Delivery of mirror image polypeptides into cells, Chem. Sci. 6 (1) (2015) 648–653.

[8] A.E. Rabideau, B.L. Pentelute, Delivery of non-native cargo into mammalian cells using anthrax lethal toxin, ACS Chem. Biol. 11 (6) (2016) 1490–1501.

[9] H.D. Herce, D. Schumacher, A.F.L. Schneider, A.K. Ludwig, F.A. Mann, M. Fillies, M.A. Kasper, S. Reinke, E. Krause, H. Leonhardt, M.C. Cardoso, C.P. R. Hackenberger, Cell-permeable nanobodies for targeted immunolabelling and antigen manipulation in living cells, Nat. Chem. 9 (8) (2017) 762–771.

[10] L. Peraro, J.A. Kritzer, Emerging methods and design principles for cell-penetrant peptides, Angew Chem. Int. Ed. Engl. 57 (37) (2018) 11868–11881.

[11] G. Appiah Kubi, Z. Qian, S. Amiar, A. Sahni, R.V. Stahelin, D. Pei, Non-peptidic cell-penetrating motifs for mitochondrion-specific cargo delivery, Angew Chem. Int. Ed. Engl. 57 (52) (2018) 17183–17188.

[12] S.R. Jean, M. Ahmed, E.K. Lei, S.P. Wisnovsky, S.O. Kelley, Peptide-mediated delivery of chemical probes and therapeutics to mitochondria, Acc. Chem. Res. 49 (9) (2016) 1893–1902.

[13] J. Yan, W. He, S. Yan, F. Niu, T. Liu, B. Ma, Y. Shao, Y. Yan, G. Yang, W. Lu, Y. Du, B. Lei, P.X. Ma, Self-assembled peptide–lanthanide nanoclusters for safe tumor therapy: overcoming and utilizing biological barriers to peptide drug delivery, ACS Nano 12 (2) (2018) 2017–2026.

[14] J. Yan, F. Ji, S. Yan, W. You, F. Ma, F. Li, Y. Huang, W. Liu, W. He, A general-purpose nanohybrid fabricated by polymeric Au(I)-Peptide precursor to wake the function of peptide therapeutics, Theranostics 10 (19) (2020) 8513–8527.

[15] F. Niu, J. Yan, B. Ma, S. Li, Y. Shao, P. He, W. Zhang, W. He, P.X. Ma, W. Lu, Lanthanide-doped nanoparticles conjugated with an anti-CD33 antibody and a p53-activating peptide for acute myeloid leukemia therapy, Biomaterials 167 (2018) 132–142.

[16] X. Wang, X. Yu, X. Wang, M. Qi, J. Pan, Q. Wang, One-step nanosurface self-assembly of d-peptides renders bubble-free ultrasound theranostics, Nano Lett. 19 (4) (2019) 2251–2258.

[17] B.P. Shah, N. Pasquale, G. De, T. Tan, J. Ma, K.B. Lee, Core-shell nanoparticle-based peptide therapeutics and combined hyperthermia for enhanced cancer cell apoptosis, ACS Nano 8 (9) (2014) 9379–9387.

[18] S.-L. Qiao, Y. Ma, Y. Wang, Y.-X. Lin, H.-W. An, L.-L. Li, H. Wang, General approach of stimuli-induced aggregation for monitoring tumor therapy, ACS Nano 11 (7) (2017) 7301–7311.

[19] J. Wan, P.F. Alewood, Peptide-decorated dendrimers and their bioapplications, Angew Chem. Int. Ed. Engl. 55 (17) (2016) 5124–5134.

[20] D.J. Peeler, S.N. Thai, Y. Cheng, P.J. Horner, D.L. Sellers, S.H. Pun, pH-sensitive polymer micelles provide selective and potentiated lytic capacity to venom peptides for effective intracellular delivery, Biomaterials 192 (2019) 235–244.

[21] I. Conejos-Sánchez, I. Cardoso, M.J. Saraiva, M.J. Vicent, Targeting a rare amyloidotic disease through rationally designed polymer conjugates, J. Contr. Release 178 (2014) 95–100.

[22] G.Y. Berguig, A.J. Convertine, S. Frayo, H.B. Kern, E. Procko, D. Roy, S. Srinivasan, D.H. Margineantu, G. Booth, M.C. Palanca-Wessels, D. Baker, D. Hockenbery, O. W. Press, P.S. Stayton, Intracellular delivery system for antibody-peptide drug conjugates, Mol. Ther. 23 (5) (2015) 907–917.

[23] T. Suma, J. Cui, M. Müllner, S. Fu, J. Tran, K.F. Noi, Y. Ju, F. Caruso, Modulated fragmentation of proapoptotic peptide nanoparticles regulates cytotoxicity, J. Am. Chem. Soc. 139 (11) (2017) 4009–4018.

[24] K. Han, J. Zhang, W. Zhang, S. Wang, L. Xu, C. Zhang, X. Zhang, H. Han, Tumor-triggered geometrical shape switch of chimeric peptide for enhanced in vivo tumor internalization and photodynamic therapy, ACS Nano 11 (3) (2017) 3178–3188.

[25] K. Cheng, Y. Ding, Y. Zhao, S. Ye, X. Zhao, Y. Zhang, T. Ji, H. Wu, B. Wang, G. J. Anderson, L. Ren, G. Nie, Sequentially responsive therapeutic peptide assembling nanoparticles for dual-targeted cancer immunotherapy, Nano Lett. 18 (5) (2018) 3250–3258.

[26] B. Sun, K. Tao, Y. Jia, X. Yan, Q. Zou, E. Gazit, J. Li, Photoactive properties of supramolecular assembled short peptides, Chem. Soc. Rev. 48 (16) (2019) 4387–4400.

[27] M. Abbas, Q. Zou, S. Li, X. Yan, Self-assembled peptide- and protein-based nanomaterials for antitumor photodynamic and photothermal therapy, Adv. Mater. 29 (12) (2017) 1605021.

[28] S. Li, Q. Zou, R. Xing, T. Govindaraju, R. Fakhrullin, X. Yan, Peptide-modulated self-assembly as a versatile strategy for tumor supramolecular nanotheranostics, Theranostics 9 (11) (2019) 3249–3261.

[29] G. Rong, C. Wang, L. Chen, Y. Yan, Y. Cheng, Fluoroalkylation promotes cytosolic peptide delivery, Sci. Adv. 6 (33) (2020), eaaz1774.

[30] B.C. Evans, R.B. Fletcher, K.V. Kilchrist, E.A. Dailing, A.J. Mukalel, J.M. Colazo, M. Oliver, J. Cheung-Flynn, C.M. Brophy, J.W. Tierney, J.S. Isenberg, K. D. Hankenson, K. Ghimire, C. Lander, C.A. Gersbach, C.L. Duvall, An anionic, endosome-escaping polymer to potentiate intracellular delivery of cationic peptides, biomacromolecules, and nanoparticles, Nat. Commun. 10 (1) (2019) 5012.

[31] B.C. Evans, K.M. Hocking, K.V. Kilchrist, E.S. Wise, C.M. Brophy, C.L. Duvall, Endosomolytic nano-polyplex platform technology for cytosolic peptide delivery to inhibit pathological vasoconstriction, ACS Nano 9 (6) (2015) 5893–5907.

[32] H. Chang, J. Lv, X. Gao, X. Wang, H. Wang, H. Chen, X. He, L. Li, Y. Cheng, Rational design of a polymer with robust efficacy for intracellular protein and peptide delivery, Nano Lett. 17 (3) (2017) 1678–1684.

[33] J. Lv, C. Liu, K. Lv, H. Wang, Y. Cheng, Boronic acid-rich dendrimer for efficient intracellular peptide delivery, Sci. China Mater. 63 (4) (2020) 620–628.

[34] G. Li, Q. Lei, F. Wang, D. Deng, S. Wang, L. Tian, W. Shen, Y. Cheng, Z. Liu, S. Wu, Fluorinated polymer mediated transmucosal peptide delivery for intravesical instillation therapy of bladder cancer, Small 15 (25) (2019), e1900936.

[35] Z. Zhang, W. Shen, J. Ling, Y. Yan, J. Hu, Y. Cheng, The fluorination effect of fluoroamphiphiles in cytosolic protein delivery, Nat. Commun. 9 (1) (2018) 1377.

[36] J. Lv, B. He, J. Yu, Y. Wang, C. Wang, S. Zhang, H. Wang, J. Hu, Q. Zhang, Y. Cheng, Fluoropolymers for intracellular and in vivo protein delivery, Biomaterials 182 (2018) 167–175.

[37] J. Lv, Y. Cheng, Fluoropolymers in biomedical applications: state-of-the-art and future perspectives, Chem. Soc. Rev. 50 (9) (2021) 5435–5467.

[38] J. Xu, J. Lv, Q. Zhuang, Z. Yang, Z. Cao, L. Xu, P. Pei, C. Wang, H. Wu, Z. Dong, Y. Chao, C. Wang, K. Yang, R. Peng, Y. Cheng, Z. Liu, A general strategy towards personalized nanovaccines based on fluoropolymers for post-surgical cancer immunotherapy, Nat. Nanotechnol. 15 (12) (2020) 1043–1052.

[39] S. Zhang, J. Shen, D. Li, Y. Cheng, Strategies in the delivery of Cas9 ribonucleoprotein for CRISPR/Cas9 genome editing, Theranostics 11 (2) (2021) 614–648.

[40] J. Lv, Q. Fan, H. Wang, Y. Cheng, Polymers for cytosolic protein delivery, Biomaterials 218 (2019) 119358.

[41] Y. Cheng, Design of polymers for intracellular protein and peptide delivery, Chin. J. Chem. 39 (2021) 1443–1449.

[42] H. Block, B. Maertens, A. Spriestersbach, N. Brinker, J. Kubicek, R. Fabis, J. Labahn, F. Schäfer, Immobilized-metal affinity chromatography (IMAC): a review, Methods Enzymol. 463 (2009) 439–473.

[43] L. Ren, J. Lv, H. Wang, Y. Cheng, A coordinative dendrimer achieves excellent efficiency in cytosolic protein and peptide delivery, Angew Chem. Int. Ed. Engl. 59 (12) (2020) 4711–4719.

[44] R. Zou, Q. Wang, J. Wu, J. Wu, C. Schmuck, H. Tian, Peptide self-assembly triggered by metal ions,, Chem. Soc. Rev. 44 (15) (2015) 5200–5219.

[45] N.A. Tavenor, M.J. Murnin, W.S. Horne, Supramolecular metal-coordination polymers, nets, and frameworks from synthetic coiled-coil peptides, J. Am. Chem. Soc. 139 (6) (2017) 2212–2215.

[46] X. Liu, F. Kang, C. Hu, L. Wang, Z. Xu, D. Zheng, W. Gong, Y. Lu, Y. Ma, J. Wang, A genetically encoded photosensitizer protein facilitates the rational design of a miniature photocatalytic CO2-reducing enzyme, Nat. Chem. 10 (12) (2018) 1201–1206.

[47] E. Borré, J.F. Stumbé, S. Bellemin-Laponnaz, M. Mauro, Light-powered self-healable metallosupramolecular soft actuators, Angew Chem. Int. Ed. Engl. 55 (4) (2016) 1313–1317.

[48] M. Kalek, A.S. Madsen, J. Wengel, Effective modulation of DNA duplex stability by reversible transition metal complex formation in the minor groove, J. Am. Chem. Soc. 129 (30) (2007) 9392–9400.

[49] S. Svenson, D.A. Tomalia, Dendrimers in biomedical applications–reflections on the field, Adv. Drug Deliv. Rev. 57 (15) (2005) 2106–2129.

[50] A.R. Menjoge, R.M. Kannan, D.A. Tomalia, Dendrimer-based drug and imaging conjugates: design considerations for nanomedical applications, Drug Discov. Today 15 (5–6) (2010) 171–185.

[51] R.M. Kannan, E. Nance, S. Kannan, D.A. Tomalia, Emerging concepts in dendrimer-based nanomedicine: from design principles to clinical applications, J. Intern. Med. 276 (6) (2014) 579–617.

[52] K. Liaw, R. Sharma, A. Sharma, S. Salazar, S. Appiani La Rosa, R.M. Kannan, Systemic dendrimer delivery of triptolide to tumor-associated macrophages improves anti-tumor efficacy and reduces systemic toxicity in glioblastoma, J. Contr. Release 329 (2021) 434–444.

[53] R. Sharma, S.P. Kambhampati, Z. Zhang, A. Sharma, S. Chen, E.I. Duh, S. Kannan, M.O.M. Tso, R.M. Kannan, Dendrimer mediated targeted delivery of sinomenine for the treatment of acute neuroinflammation in traumatic brain injury, J. Contr. Release 323 (2020) 361–375.

[54] P. Sinha, A.K. Sonkar, K. Tripathi, N. Kumari, L. Mishra, Metalloreceptors of the type L-M-L [L=(4' -(2-pyridyl)-2,2' :6',2'' -terpyridine), M=Co(II), Cu(II), Zn(II)] for the recognition of Fe^{2+} ions, Polyhedron 134 (2017) 192–198.

[55] Y. Gao, D. Rajwar, A.C. Grimsdale, Self-assembly of conjugated units using metal-terpyridine coordination, Macromol. Rapid Commun. 35 (2014) 1727–1740.

[56] R. Shunmugam, G.J. Gabriel, K.A. Aamer, G.N. Tew, Metal-ligand-containing polymers: terpyridine as the supramolecular unit, Macromol. Rapid Comm. 31 (9–10) (2010) 784–793.

[57] H. Hofmeier, U.S. Schubert, Recent developments in the supramolecular chemistry of terpyridine-metal complexes, Chem. Soc. Rev. 33 (6) (2004) 373–399.

[58] S.N. Karuk Elmas, Z.E. Dincer, A.S. Erturk, A. Bostanci, A. Karagoz, M. Koca, G. Sadi, I. Yilmaz, A novel fluorescent probe based on isocoumarin for Hg^{2+} and Fe^{3+} ions and its application in live-cell imaging, Spectrochim. Acta 224 (2020) 117402.

[59] H. Zhang, J. Yang, K. Liang, J. Li, L. He, X. Yang, S. Peng, X. Chen, C. Ding, J. Li, Effective dentin restorative material based on phosphate-terminated dendrimer as artificial protein, Colloid. Surface. B 128 (2015) 304–314.

[60] K.S. Finnie, J.R. Bartlett, J.L. Woolfrey, Vibrational spectroscopic study of the coordination of (2,2'-bipyridyl-4,4'-dicarboxylic acid) ruthenium(II) complexes to the surface of nanocrystalline titania, Langmuir 14 (10) (1998) 2744–2749.

[61] D. Wang, H. Wang, H. Li, Novel luminescent soft materials of terpyridine-containing ionic liquids and europium(III), ACS Appl. Mater. Interfaces 5 (13) (2013) 6268–6275.

[62] F.E. Sarac Oztuna, M.B. Yagci, U. Unal, First-row transition-metal cations (Co^{2+}, Ni^{2+}, Mn^{2+}, Fe^{2+}) and graphene (oxide) composites: from structural properties to electrochemical applications, Chemistry 25 (12) (2019) 3131–3140.

[63] M. Zhang, L. Zhu, C. He, X. Xu, Z. Duan, S. Liu, M. Song, S. Song, J. Shi, Y. Li, G. Cao, Adsorption performance and mechanisms of Pb(II), Cd(II), and Mn(II) removal by a β-cyclodextrin derivative, Environ. Sci. Pollut. Res. 26 (5) (2019) 5094–5110.

[64] T. Tsukamoto, K. Takada, R. Sakamoto, R. Matsuoka, R. Toyoda, H. Maeda, T. Yagi, M. Nishikawa, N. Shinjo, S. Amano, T. Iokawa, N. Ishibashi, T. Oi, K. Kanayama, R. Kinugawa, Y. Koda, T. Komura, S. Nakajima, R. Fukuyama, N. Fuse, M. Mizui, M. Miyasaki, Y. Yamashita, K. Yamada, W. Zhang, R. Han, W. Liu, T. Tsubomura,

H. Nishihara, Coordination nanosheets based on terpyridine–zinc(II) complexes: as photoactive host materials, J. Am. Chem. Soc. 139 (15) (2017) 5359–5366.

[65] R. Botár, E. Molnár, G. Trencsényi, J. Kiss, F.K. Kálmán, G. Tircsó, Stable and inert Mn(II)-Based and pH-responsive contrast agents, J. Am. Chem. Soc. 142 (4) (2020) 1662–1666.

[66] M.K. Islam, S. Kim, H.-K. Kim, S. Park, G.-H. Lee, H.J. Kang, J.-C. Jung, J.-S. Park, T.-J. Kim, Y. Chang, Manganese complex of ethylenediaminetetraacetic acid (EDTA)–Benzothiazole aniline (BTA) conjugate as a potential liver-targeting MRI contrast agent, J. Med. Chem. 60 (7) (2017) 2993–3001.

[67] M.K. Islam, S. Kim, H.K. Kim, Y.H. Kim, Y.M. Lee, G. Choi, A.R. Baek, B.K. Sung, M. Kim, A.E. Cho, H. Kang, G.H. Lee, S.H. Choi, T. Lee, J.A. Park, Y. Chang, Synthesis and evaluation of manganese(II)-Based ethylenediaminetetraacetic acid-ethoxybenzyl conjugate as a highly stable hepatobiliary magnetic resonance imaging contrast agent, Bioconjugate Chem. 29 (11) (2018) 3614–3625.

[68] M. Huang, Y. Zhang, W. Xiang, T. Zhou, X. Wu, J. Mao, Efficient adsorption of Mn (II) by layered double hydroxides intercalated with diethylenetriaminepentaacetic acid and the mechanistic study, J. Environ. Sci. (China) 85 (2019) 56–65.

[69] S. Pan, Y. Zhang, H. Shen, M. Hu, An intensive study on the magnetic effect of mercapto-functionalized nano-magnetic Fe_3O_4 polymers and their adsorption mechanism for the removal of Hg(II) from aqueous solution, Chem. Eng. J. 210 (2012) 564–574.

[70] S. Shoji-Kawata, R. Sumpter, M. Leveno, G.R. Campbell, Z. Zou, L. Kinch, A. D. Wilkins, Q. Sun, K. Pallauf, D. MacDuff, C. Huerta, H.W. Virgin, J.B. Helms, R. Eerland, S.A. Tooze, R. Xavier, D.J. Lenschow, A. Yamamoto, D. King, O. Lichtarge, N.V. Grishin, S.A. Spector, D.V. Kaloyanova, B. Levine, Identification of a candidate therapeutic autophagy-inducing peptide, Nature 494 (7436) (2013) 201–206.

[71] S. Wu, Y. He, X. Qiu, W. Yang, W. Liu, X. Li, Y. Li, H.M. Shen, R. Wang, Z. Yue, Y. Zhao, Targeting the potent Beclin 1-UVRAG coiled-coil interaction with designed peptides enhances autophagy and endolysosomal trafficking, Proc. Natl. Acad. Sci. U. S. A. 115 (25) (2018) E5669–E5678.

[72] L. Peraro, Z. Zou, K.M. Makwana, A.E. Cummings, H.L. Ball, H. Yu, Y.S. Lin, B. Levine, J.A. Kritzer, Diversity-oriented stapling yields intrinsically cell-penetrant inducers of autophagy, J. Am. Chem. Soc. 139 (23) (2017) 7792–7802.

[73] Y. Wang, Y.X. Lin, Z.Y. Qiao, H.W. An, S.L. Qiao, L. Wang, R.P. Rajapaksha, H. Wang, Self-assembled autophagy-inducing polymeric nanoparticles for breast cancer interference in-vivo, Adv. Mater. 27 (16) (2015) 2627–2634.

[74] Z. Zhou, Y. Yan, L. Wang, Q. Zhang, Y. Cheng, Melanin-Like nanoparticles decorated with an autophagy-inducing peptide for efficient targeted photothermal therapy, Biomaterials 203 (2019) 63–72.

[75] S. Wang, F. Li, R. Qiao, X. Hu, H. Liao, L. Chen, J. Wu, H. Wu, M. Zhao, J. Liu, R. Chen, X. Ma, D. Kim, J. Sun, T.P. Davis, C. Chen, J. Tian, T. Hyeon, D. Ling, Arginine-rich manganese silicate nanobubbles as a ferroptosis-inducing agent for tumor-targeted theranostics, ACS Nano 12 (12) (2018) 12380–12392.

[76] L.S. Lin, J. Song, L. Song, K. Ke, Y. Liu, Z. Zhou, Z. Shen, J. Li, Z. Yang, W. Tang, G. Niu, H.H. Yang, X. Chen, Simultaneous fenton-like ion delivery and glutathione depletion by MnO_2 -based nanoagent to enhance chemodynamic therapy, Angew Chem. Int. Ed. Engl. 57 (18) (2018) 4902–4906.

[77] C. Wang, Y. Guan, M. Lv, R. Zhang, Z. Guo, X. Wei, X. Du, J. Yang, T. Li, Y. Wan, X. Su, X. Huang, Z. Jiang, Manganese increases the sensitivity of the cGAS-STING pathway for double-stranded DNA and is required for the host defense against DNA viruses, Immunity 48 (4) (2018) 675–687, e7.